



OPEN

Dual-energy computed tomography as a lower radiation dose alternative to perfusion computed tomography in tumor viability assessment

Arkadiusz Zegadło¹, Aleksandra Różyk¹, Magdalena Żabicka¹, Ewa Więsik-Szewczyk² & Artur Maliborski¹

To present the utility of dual-energy computed tomography (DECT) in the assessment of angiogenesis of focal lesions as an example of a solitary pulmonary nodule (SPN). This prospective study comprised 28 patients with SPN who underwent DECT and perfusion computed tomography (CTP), according to a proprietary protocol. Two radiologists independently analyzed four perfusion parameters, namely blood flow (BF), blood volume (BV), the time to maximum of the tissue residue function (Tmax), permeability surface area product (PS) from CTP, in addition to the iodine concentration (IC) and normalized iodine concentration (NIC) of the SPN from DECT. We used the Pearson R correlation and interclass correlation coefficients (ICC_s). Statistical significance was assumed at $p < 0.05$. The mean tumor size was 23.5 ± 6.5 mm. We observed good correlations between IC and BF ($r = 0.78$, $p < 0.000$) and NIC and BF ($r = 0.71$, $p < 0.000$) as well as between IC and BV ($r = 0.73$, $p < 0.000$) and NIC and BV ($r = 0.73$, $p < 0.000$) and poor correlation between IC and PS ($r = 0.38$, $p = 0.044$). There was no correlation between NIC and PS ($r = 0.35$, $p = 0.064$), IC content and Tmax ($r = -0.28$, $p = 0.147$) and NIC and Tmax ($r = -0.21$, $p = 0.266$). Inter-reader agreement on quantitative parameters at CTP (ICC_{PS} = 0.97, ICC_{Tmax} = 0.96, ICC_{BV} = 0.98, and ICC_{BF} = 0.99) and DECT (ICC_{IC} = 0.98) were excellent. The radiation dose was significantly lower in DECT than that in CTP (4.84 mSv vs. 9.07 mSv, respectively). DECT is useful for the functional assessment of oncological lesions with less exposure to radiation compared to perfusion computed tomography.

Abbreviations

BF	Blood flow
BV	Blood volume
CTDI _{vol}	Volume computed tomography dose index
CT	Computed tomography
CTP	Perfusion computed tomography
DECT	Dual Energy Computed Tomography
DLP	Dose length product
IC	Iodine concentration
NIC	Normalized iodine concentration
PS	Permeability surface area product
ROI	Region of interest
SPN	Solitary pulmonary nodule
Tmax	Time-to-maximum of the tissue residue function

¹Department of Radiology, Military Institute of Medicine- National Research Institute, Szaserów 128, 04-141 Warsaw, Poland. ²Department of Internal Medicine, Pulmonology, Allergy and Clinical Immunology, Central Clinical Hospital of the Ministry of National Defense, Military Institute of Medicine-National Research Institute, Warsaw, Poland. ✉email: arozyk@wim.mil.pl

TU Tumor
VEGF Vascular endothelial growth factor

Of 14 million malignant tumors diagnosed worldwide in 2012, approximately 13% (1.8 million) were lung cancers. They are the most common malignant neoplastic disease in the men (16.7%) and the third most common disease in women (8.7%), following breast cancer and colorectal cancer¹. Current multimodal treatment strategies utilizing induction chemotherapy or radiotherapy increase the number of patients undergoing a surgical resection of the tumor. They are extremely effective for patients with early stage lung cancer. The 5-year survival rate of patients with early surgical resection is 60–80%². In contrast, patients with advanced lung cancer have an unfavorable prognosis, with a 5-year survival rate of 7–15%^{2,3}. Computed tomography (CT) is often the first examination performed to detect lung tumors in imaging tests⁴.

Tumor angiogenesis is a key component of tumor diagnosis and treatment. Neovascularization-mediated tumor enhancement by $> +20$ Hounsfield units (HU)^{5,6} indicates malignancy, and is an important criterion for the differentiation of lesions^{7–9}. The vascularization of pulmonary lesions is complex. Primary bronchial carcinomas are principally nourished by bronchial circulation; however, in several cases, the vascularization component of the pulmonary artery is present and grows for tumors around the periphery of the lung¹⁰. The degree of tumor vessel development, the degree of organization of their network, and the permeability to the tumor matrix determine the anti-angiogenic treatment strategy¹¹.

Perfusion computed tomography (CTP) is a dynamic test that enables the *in vivo* assessment of the viability and degree of vascularization of the tumor, which affects the diagnosis, staging assessment, prognosis, and monitoring of the response to anti-angiogenic treatment^{12–17}. Tumor microvessel density, as measured by the microvessel density (MVD) value, and vascular endothelial growth factor (VEGF) expression, as assessed by histopathology, are positively correlated with the results of the solitary pulmonary nodule (SPN) CTP examination. This confirms the significance of CTP as a specific biomarker in imaging for monitoring the effects of chemotherapy and radiotherapy^{18,19}. CTP is a dynamic and volumetric examination that includes multiple scans of a designated area in a fixed time span. Therefore, it comprises the mean radiation dose of CTP for chest 1.5 times higher than the dose of the routinely used CT protocol for chest examination (1288.8 mGy cm vs. 885.2 mGy cm, respectively)²⁰.

Dual-energy CT (DECT) examination enables the quantification of iodine concentration in selected regions of interest (ROI), thereby indirectly indicating the degree of tumor vascularization. It is based on images dependent on the distribution of iodine in the examined tissues. Previous studies have reported on the usefulness of assessing images dependent on the concentration of iodine in DECT, compared to perfusion images^{21–23}.

We aimed to evaluate the possibility of using a single DECT scan as an alternative to high-dose CTP for assessing solid lung lesion angiogenesis, which we believe could be particularly beneficial for oncology patients, who often require multiple periodic follow-up CT scans.

Materials and methods

This prospective study was approved by the Bioethics Committee of the Military Institute of Medicine in Warsaw, Poland on January 22, 2020 (protocol code 1/WIM/2020) and was conducted in accordance with the Declaration of Helsinki. All patients were informed about the conditions of participation in the study and provided their written informed consent.

Patients. Between February 2020 and December 2020, we enrolled 70 patients aged ≤ 80 years who were hospitalized for further diagnosis and the treatment of a lung lesion, with a longitudinal size ≤ 30 mm. Patients with contrast medium hypersensitivity ($n=3$), pregnancy ($n=0$), glomerular filtration rate (GFR) < 60 ml/min/kg ($n=15$), the refusal to undergo a double CT scan in the combined protocol (CTP + DECT) ($n=4$), and anxiety responses ($n=2$) were excluded from the study. Eventually, 46 patients underwent combined scanning (CTP + DECT) in accordance with our protocol. Of these patients, 18 were excluded from the analysis because of excessive respiratory mobility causing a part of the tumor to be moved out of the scan range ($n=6$), the lack of reliable perfusion data ($n=7$), and the lack of definitive histopathological diagnosis ($n=5$). Eventually, 28 patients were included in the analysis (Fig. 1).

CT protocol. All patients underwent a dynamic and polychromatic perfusion examination of the lung tumor. Five minutes later, the DECT examination was performed according to a self-designed protocol. The DECT examination were performed using a single-source DECT scanner with rapid kVp switching Discovery CT 750 HD (GE Healthcare, WI, USA). Before scanning, the subjects were instructed on the breathing method necessary to reduce motion blurring artifacts.

First, to determine the position of the SPN, we performed a native, helical chest scan, including diaphragm domes according to the following parameters: tube voltage, 120 kVp; current time product, 630 mAs; slice thickness 2.5 mm, and scanner rotation time 0.6 s.

After determining the tumor location, we performed a dynamic, axial CTP examination with a length of 40 mm (z-axis), which covered the area of the lesion with an unmoved scanner table according to the following protocol: tube voltage 80 kVp, current time product 100 mAs, large field of view (SFOV) 50 cm, slice thickness 5.0 mm and scanner rotation time 2 s. A bolus of 50 ml of non-ionic iodine contrast (400 mg/ml Iomeron, Bracco Imaging Deutschland GmbH, Konstanz, Germany) was used for CTP from an access through the cephalic vein at a rate of 5 ml/s, by injecting it with 20 ml of saline solution at a similar speed. In CTP, 30 scans were captured during a 60 s exposure at 2 s intervals. The beginning of the contrast agent bolus and the onset of CTP were simultaneous. The end of the contrast bolus was at the 10th second of the perfusion scan (Fig. 2).

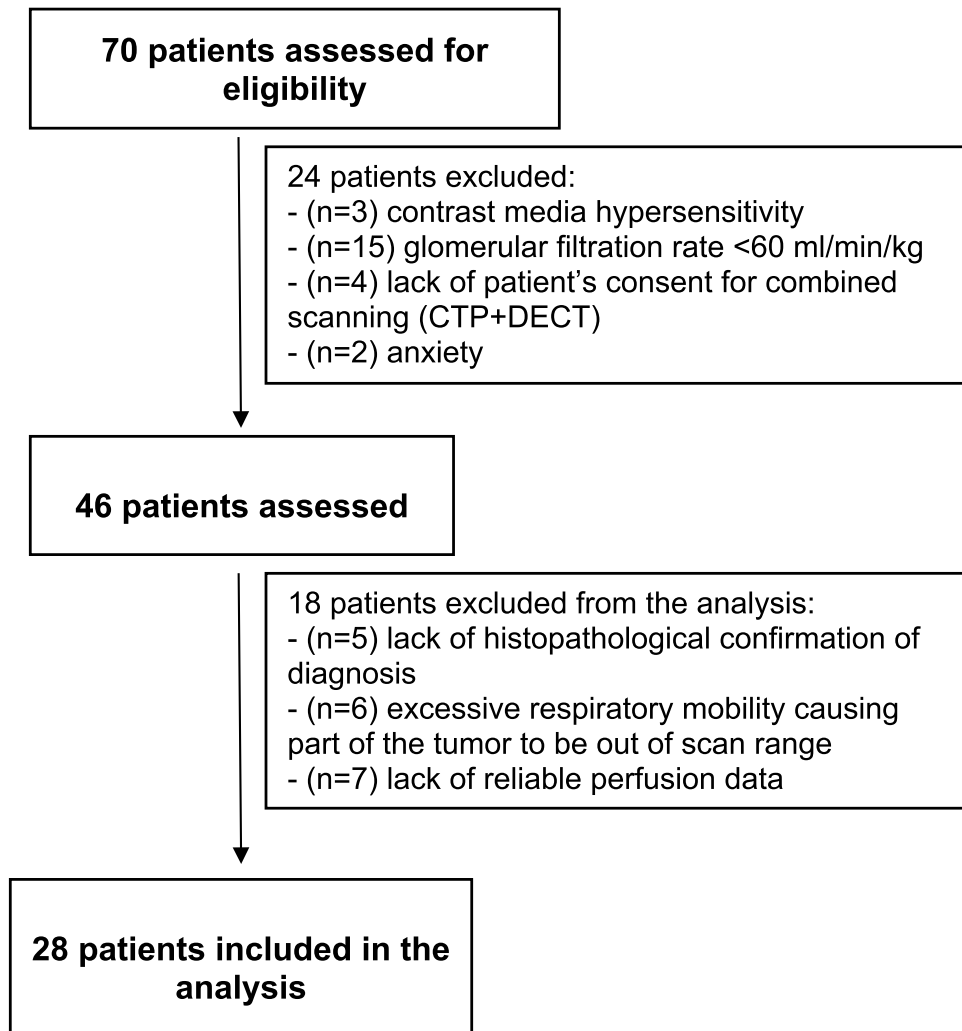


Figure 1. Inclusion and exclusion criteria for patient selection.

The DECT phase was delayed by 300 s after the CTP phase. Moreover, it covered the similar tumor range according to the following protocol: tube voltage 70 kVp (range 80–140 kVp); tube current ~260 mA (modulated); scan time per rotation 0.8 s, large field of view (SFOV) 50 cm; slice thickness 1.25 mm; and detector collimation 64×0.625 mm. DECT involved the iodine contrast similar to that used in CTP at different doses depending on the body weight at a rate of 5 ml/s, injected by a bolus of 20 ml of saline solution. We used the following formula:

$$\text{The amount of contrasti.v.} = [(2 \text{ ml}/1 \text{ kg}) - 50 \text{ ml}].$$

The scanning was initiated when the concentration of the contrast agent in the thoracic aorta exceeded 100 HU (Fig. 3).

The images were reconstructed to a thickness of 5 mm for comparison with CTP images (Table 1).

The radiation doses absorbed separately from dynamic CTP and DECT scanning were reported as two parameters, namely the dose length product (DLP, mGy-cm) and volume dose index (CTDIvol, mGy). The effective dose was calculated by multiplying the DLP with the conversion factor $0.0014 \text{ mSv}/\text{mGy}^{-1} \text{ cm}^{-1}$.

Perfusion CT and DECT quantitative analysis. All combined CTP and DECT studies were sent from the scanner to the commercially available Advantage Workstation 4.7 (GE Healthcare). We analyzed the CTP images using the software CT perfusion 4D, GE Healthcare, based on the deconvolution method²⁴. The studies were independently assessed by two radiologists AZ and MZ with 17 and 27 years of experience in imaging lung pathology, respectively. The software automatically calculated the four perfusion parameters as follows: blood flow (BF) (ml/100 g/min), blood volume (BV) (ml/100 g), time-to-maximum of the tissue residue function (Tmax) (s), and permeability surface area product (PS) (ml/100 g/min) (Fig. 4).

Same radiologists performed the DECT examinations according to the Gemstone Spectral Imaging (GSI) General protocol in the GE Healthcare software Advantage Workstation 4.7. ROI measurement locations were manually based on similar areas marked independently in CTP measurements, and were performed with the

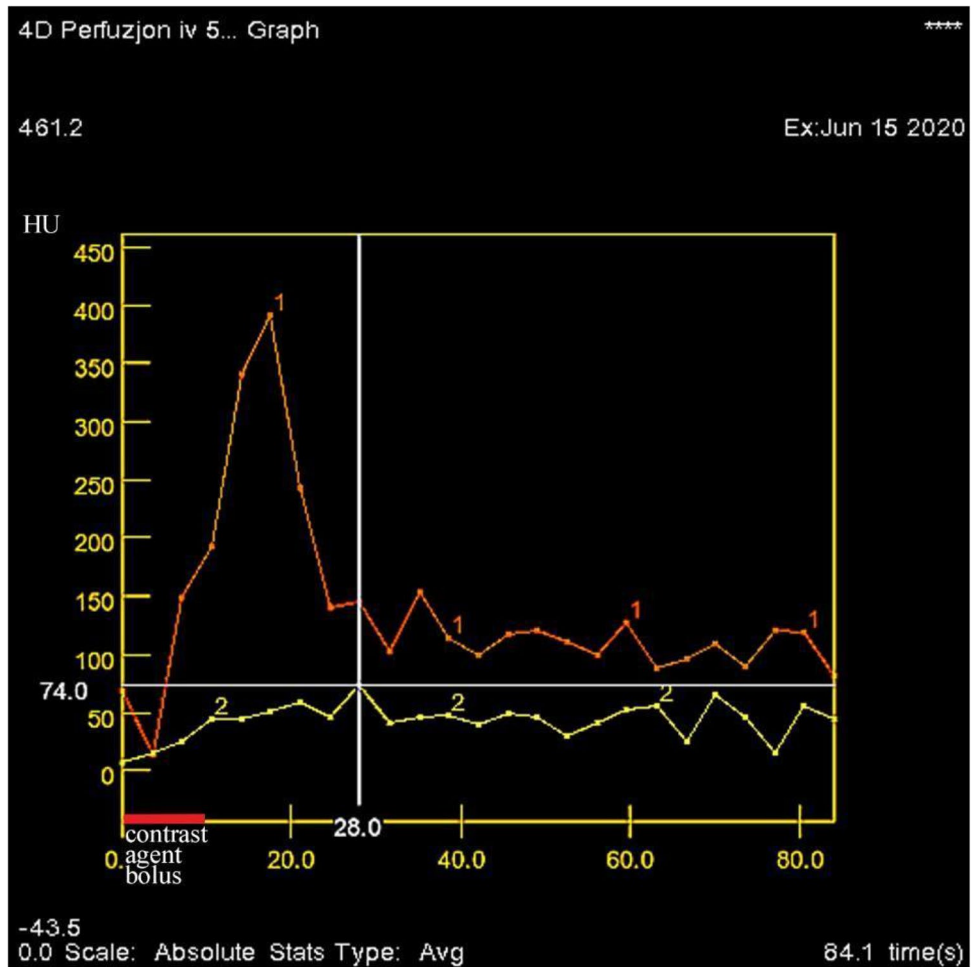


Figure 2. An example of CTP scanning. The contrast enhancement of the aorta is marked in red and the flow in the SPN is marked in yellow. The contrast bolus lasts for 10 s and begins simultaneously with the commencement of the scan. The greatest contrast enhancement of the tumor to +74 HU is observed 28 s after contrast administration. *CTP* perfusion computed tomography.

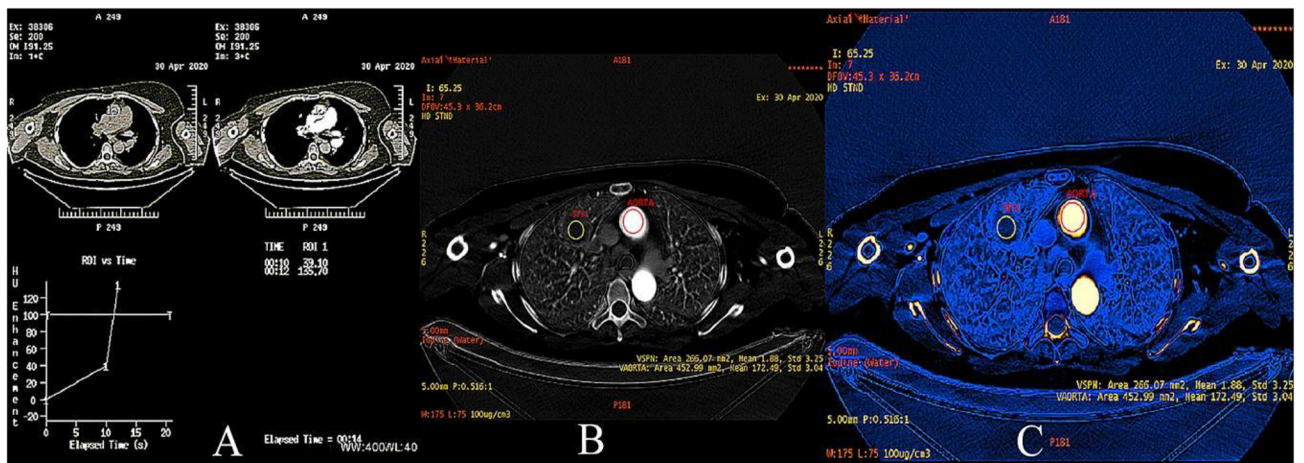


Figure 3. Exceeding the density of 100 HU in the ROI in the ascending aorta initiates the DECT (A) scan. Presentation of iodine concentrations at the reference site on the Linear Gray map (B) scan and the Color map (C) scan. DECT (ascending aorta—red ROI) and in the lung tumor (SPN—yellow ROI). Iodine concentration in the aorta and lung focal lesion is $172.49 \times 100 \mu\text{g}/\text{cm}^3$ and $1.88 \times 100 \mu\text{g}/\text{cm}^3$, respectively. *DECT* dual-energy computed tomography, *SPN* solitary pulmonary nodule, *ROI* region of interest.

Phase	Tube potential	Tube current (mAs)	Rotation time (s)	Detector coverage (mm)	Slice thickness (mm)	Pitch/speed (mm/rot)	DLP (mGy-cm)	Total exposure time (s)	CTDI _{vol} (mGy)	Number of acquisitions	Matrix size (mm)	DFOV
I Native	120 kVp	630	0.6	40	2.5	1.375:1/55.00	–	5.18	–	Helical	512 × 512	Large (50 cm)
Contrast agent: 50 ml (flow 5 ml/s, bolus time 10 s)												
II CTP	80 kVp	100	2.0	40	5.0	–	648,61	60.0	162,15	Axial 30	512 × 512	Large (50 cm)
Contrast agent: [2 ml/kg–50 ml], (flow 5 ml/s); bolus tracking ROI: descending aorta, trigger threshold 100 HU												
III DECT	70 keV	~260	0.8	40	1.25	0.516:1/20.62	346,41	6.83	19,67	Helical 109	512 × 512	Large (50 cm)

Table 1. Acquisition protocol for dynamic CTP and DECT. DECT dual-energy computed tomography, CTP perfusion computed tomography, CTDI_{vol} volume dose index, DFOV display field of view.

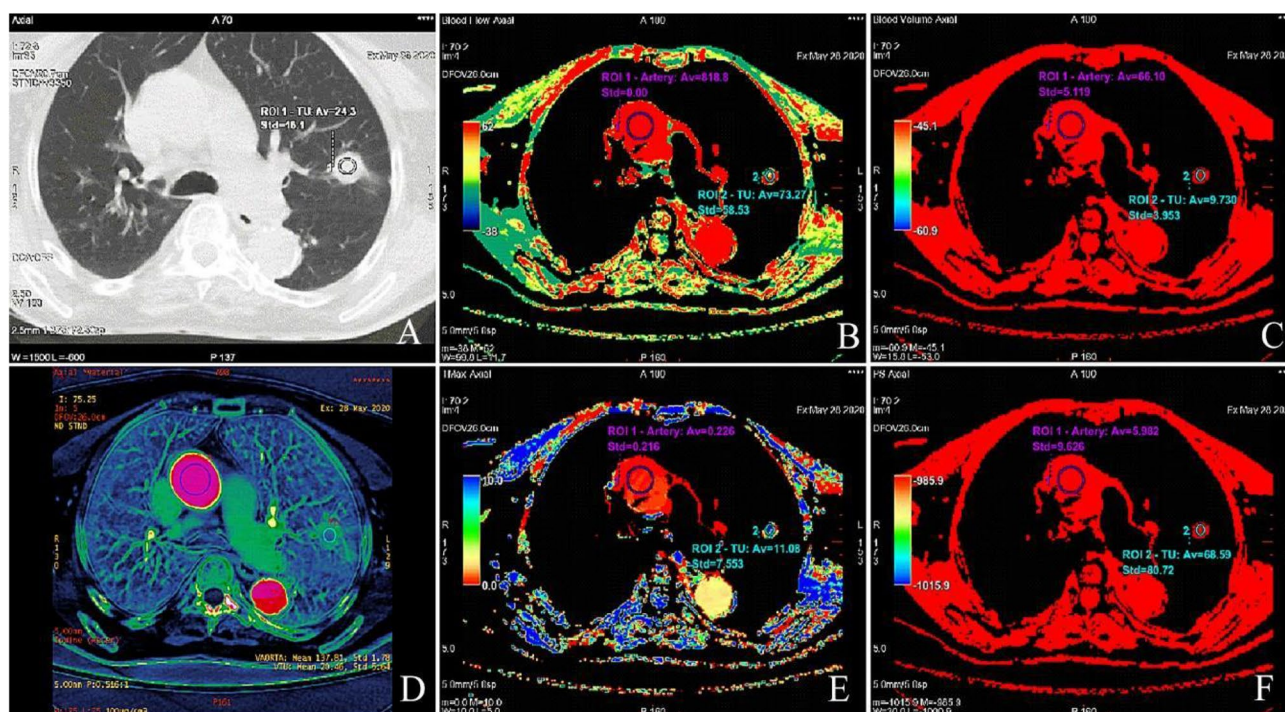


Figure 4. (A) CT scan displaying a circular ROI manually placed on the TU with average value of 24.3 HU. (B) BF 73.27 ml/100 g/min presents the mean flow rate through vasculature in the ROI tissue region of the TU. ROI 1 (purple color) represents the aorta, ROI 2 (green) denotes the tumor cross-section. (C) BV 9.73 ml/100 g presents the mean volume of flowing blood within a vasculature of the tissue region. (D) Contrast enhancement DECT reconstruction performed with Color maps French software on GE healthcare Workstation 4.7. (E) Tmax 11.08 s represents the delayed arrival of contrast bolus. (F) PS 68.59 ml/100 g/min denotes the total flux from the plasma to the interstitial space. CTP perfusion computed tomography, ROI region of interest, TU tumor, BV blood volume, BF blood flow, Tmax the time to the maximum of the residue function.

utmost care by both researchers. The results ($\times 100 \mu\text{g}/\text{cm}^3$) were read automatically, and displayed mean concentrations of the contrast agent iodine (IC) in the ROI regions corresponding to the CTP measurement sites.

Statistical analyses. We used a commercial statistical software package (Statistica w 13.3 Windows, TIBCO Software Inc., Palo Alto, USA) for statistical analyses. Continuous variables are presented as mean \pm standard deviation (SD), median, and 95% confidence interval (CI). The variables were assessed for normal distribution using the Kolmogorov–Smirnov test. We used the Pearson product–moment correlation coefficient (r) to compare the iodine concentration values and four perfusion parameters (BF, BV, Tmax, and PS) in SPNs. Interclass correlation coefficients (ICC) were assessed using the intra-reader agreement for estimating perfusion for each pair of variables. In order to minimize variation between patients, the nodule iodine concentration was normalized to IC in the aorta to derive a normalized iodine concentration (NIC) by the formula: $NIC = IC_{\text{tumor}} : IC_{\text{aorta}}$

Differences were considered statistically significant at $p < 0.05$.

Results

Patients and tumor characteristics. The 28 included patients comprised 15 women (mean age: 70 ± 10 years) and 13 men (mean age: 68.5 ± 6 years). All patients had a single lung tumor that was assessed on CTP and DECT as well as examined histopathologically. Of these tumors, 10 (36%) were adenocarcinomas, seven (25%) were squamous cell carcinoma, four (14%) were hamartomas, three were granulomas (11%), and one each (4%) comprised carcinoid tumor, large cell neuroendocrine carcinoma, pneumoconiosis, and diagnosed with hypersensitivity pneumonia (Table 2).

The mean tumor size was 23.5 ± 6.5 mm (median 26 mm, CI 5.3–9.0 mm), with a native density of $+20.5 \pm 7.7$ HU (median +20.5 HU, CI 5.9–10.2 HU). The mean SPN enhancement following contrast administration was 49.4 ± 21.9 HU (median 51.9 HU, CI 17.3–29.8 HU).

CTP and DECT quantitative analysis. Two radiologists recorded two measurements of each of the four CTP parameters as follows: PS, Tmax, BV, BF, and IC. Interreader agreement for the quantitative parameters on perfusion CT ($ICC_{PS} = 0.97$, $ICC_{Tmax} = 0.96$, $ICC_{BV} = 0.98$, and $ICC_{BF} = 0.99$) and DECT ($ICC_{IC} = 0.98$) were excellent (Koo and Li, 2016). Table 3 summarizes the quantitative parameters from DECT and CTP.

Correlations between perfusion CT (CTP) and dual-energy CT (DECT). We observed positive correlations between the concentration of iodine in the lung tumor and perfusion parameters²⁵ as follows: strong correlation for BF ($r = 0.78$, $p < 0.001$), moderate correlation for BV ($r = 0.73$, $p < 0.001$) and poor correlation between the PS values ($r = 0.39$, $p = 0.044$). We did not observe a statistically significant relationship between the iodine content in the lung tumor and Tmax ($r = -0.28$, $p = 0.147$) (Fig. 5, Table 4).

Correlations between perfusion and parameter normalized IC in lung tumors were as follows: BF ($r = 0.71$, $p < 0.000$), moderate correlation for BV ($r = 0.73$, $p < 0.000$). We did not observe a statistically significant

	N (%)	Age \pm SD (year)	Lung	Lobe (N)	Diagnosis (N)
Total	28 100%	69 \pm 9	Right	Upper 14	Adenocarcinoma 6 Granuloma 2 Squamous cell carcinoma 3 Hamartoma 2 Pneumoconiosis 1
				Middle 3	Squamous cell carcinoma 1 Carcinoid tumor 1 Hypersensitivity pneumonia 1
				Lower 5	Adenocarcinoma 2 Granuloma 1 Squamous cell carcinoma 1 Hamartoma 1
			Left	Upper 4	Adenocarcinoma 1 Squamous cell carcinoma 1 Hamartoma 1 Large cell neuroendocrine carcinoma 1
				Lower 2	Adenocarcinoma 1 Squamous cell carcinoma 1
			Female	15 54%	70 \pm 10
Middle 1	Hypersensitivity pneumonia 1				
Lower 3	Adenocarcinoma 2 Granuloma 1				
Left	Upper 3	Adenocarcinoma 1 Hamartoma 1 Large cell neuroendocrine carcinoma 1			
	Lower 2	Adenocarcinoma 1 Squamous cell carcinoma 1			
Male	13 46%	68.5 \pm 6	Right	Upper 8	Adenocarcinoma 3 Granuloma 2 Squamous cell carcinoma 2 Pneumoconiosis 1
				Middle 2	Squamous cell carcinoma 1 Carcinoid tumor 1
				Lower 2	Squamous cell carcinoma 1 Hamartoma 1
			Left	Upper 1	Squamous cell carcinoma 1
				Lower 0	0

Table 2. Characteristics of the patients, localization, and the number solid lung nodules. *N* number, *y* years, *SD* standard deviation.

Perfusion CT	Mean \pm SD	Median	CI (-95%–+95%)
PS (ml/100 g/min)	28.4 \pm 26.3	28.1	18.2–38.6
Tmax (s)	6.1 \pm 4.6	5.4	4.2–7.9
BF (ml/100 g/min)	133.1 \pm 83.7	124.7	100.7–165.6
BV (ml/100 g)	6.9 \pm 5.4	5.6	4.8–9.0
DECT			
IC ($\times 100 \mu\text{g}/\text{cm}^3$)	16.2 \pm 8.7	16.3	12.8–19.6

Table 3. Quantitative parameters from perfusion computed tomography and dual-energy computed tomography. *BF* blood flow, *BV* blood volume, *PS* permeability surface area product, *Tmax* the time-to-maximum of the tissue residue function, *SD* standard deviation, *CI* confidence interval.

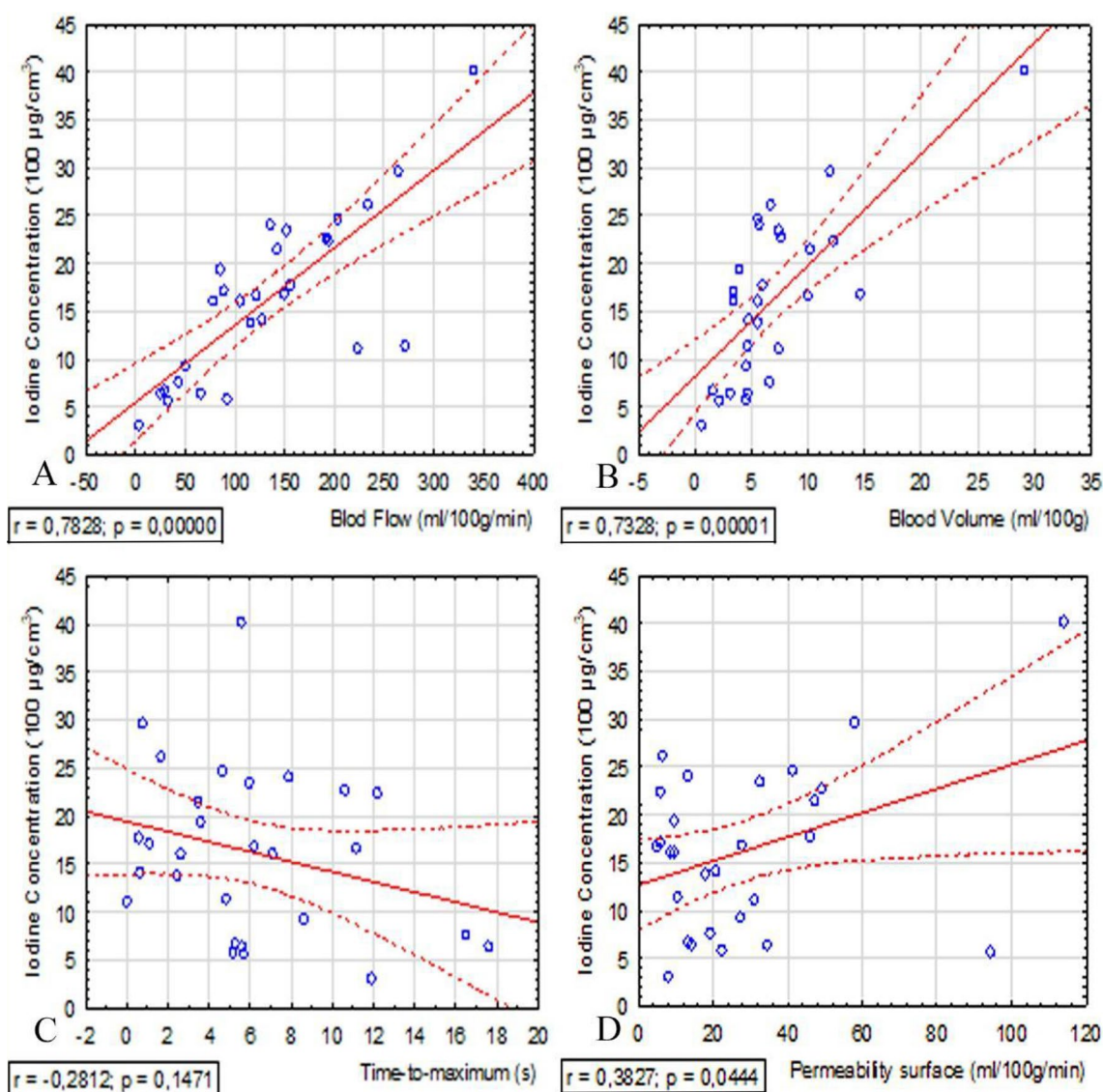


Figure 5. Scatterplot displaying Pearson correlation between the Blood Flow (A), the Blood Volume (B), the Time to maximum of the residue function (C), the Permeability surface (D) at CTP and iodine concentration at DECT in SPNs with upper and lower lines indicating 95% confidence intervals. SPNs, SPN solitary pulmonary nodule, *r* correlation coefficient, *p* statistical significance.

Correlation	r	r ²	p
BF and IC	+0.78	0.61	0.000
BV and IC	+0.73	0.53	0.000
PS and IC	+0.38	0.14	0.044
Tmax and IC	-0.28	0.08	0.147
BF and NIC	+0.71	0.53	0.000
BV and NIC	+0.73	0.53	0.000
PS and NIC	+0.35	0.12	0.064
Tmax and NIC	-0.21	0.05	0.266

Table 4. Correlations of quantitative parameters between perfusion computed tomography and dual-energy computed tomography in patients with solitary pulmonary nodule (SPN). *BF* blood flow, *BV* blood volume, *PS* permeability surface area product, *Tmax* time-to-maximum of the tissue residue function, *IC* iodine concentration, *NIC* normalized iodine concentration; R, correlation coefficient; R², square of the correlation coefficient; and P, statistical significance.

relationship between the NIC and PS values ($r=0.35$, $p=0.064$) and Tmax ($r=-0.21$, $p=0.266$). Correlation between NIC and IC was $r=0.83$, $p=0.000$.

Radiation dose. A fixed scanning protocol was used in this study. Therefore, the volumetric CT dose rate (CTDIvol) was a constant value of 162.15 mGy for each dynamic CTP scan (1 scan/2 s/60 s). However, for a single DECT scan, the dose was much lower at 19.67 mGy. Simultaneously, DLP measurements for CTP and DECT scans were 648.61 mGy-cm (9.07 mSv) and 346.41 mGy-cm (4.84 mSv), respectively (the effective dose was calculated by multiplying the DLP with the conversion factor 0.0014 mSv/mGy⁻¹ cm⁻¹).

Discussion

The DECT modality displays the accumulation of a contrast agent measured in conventional CT in HU units as its concentration in 1 cm³ of tissue, which is a unique solution. In pulmonary diagnostics it is used to assess malignancy of lung tumors^{26,27} or to differentiate the subtypes of malignant tumors²⁸, assess lung vessels²⁹⁻³¹ and lung tissue pathologies^{32,33}.

Our findings demonstrated a strong correlation between the iodine content measured on IC maps and normalized IC maps in the single source modality, fast kV-switching DECT and perfusion parameters BF ($R=0.78$ for IC and $R=0.71$ for normalized IC) and BV ($R=0.73$ for IC and $R=0.73$ for normalized IC) in the vascular bed of a lung tumor 23.5 ± 6.5 mm of size, with comparatively lower exposure to the biological effects of radiation. Furthermore, the degree of this relationship demonstrated a high level of statistical significance ($p < 0.000$). The similar results of BV in comparison to IC and normalized IC indicate that this parameter is less dependent on the method of measuring the iodine concentration on DECT maps.

This was consistent with the results of studies on hepatocellular carcinoma by Mulé et al.³⁴. In 2018, other authors³⁵ demonstrated a correlation between IC and BF measurements during the assessment of the pancreas in healthy participants and patients with cancer. In a study on colorectal cancers³³, Kang et al. indicated a relationship between perfusion parameters and the concentration of iodine in the tumor vessels with lower radiation exposure of DECT, compared to CTP. Strong correlation between the concentration of iodine on DECT maps in the arterial phase of contrast enhancement and perfusion in the hepatocellular carcinoma area²² is another example of the multidisciplinary application of DECT in the dynamic assessment of organ lesions as an alternative to PCT. Zhu et al.³⁶ used this two modalities to differentiate the benign and malignant pulmonary nodules and showed that the iodine parameters from DECT significantly correlated with BV and BF, but with lower sensitivity and specificity for IC (86, 67 and 72, 73) in DECT in comparison to BV (94, 44 and 73, 33).

Numerous authors described a correlation of both BF and BV with the biomarkers of angiogenesis, namely microvessel density (MVD) and vascular endothelial growth factor (VEGF) concentration. BV correlates with the number of vessels that display the volume of blood collected in them³⁷. The increase in tumor BF is an effect of the increase in blood flow at the arteriovenous connections that nourish the growing tumor, which translates into an assessment of tumor viability. The scale of reports appears promising and indicates the usefulness of CTP as a non-invasive technique to assess tumor viability^{12-14,38} and indicates the utility of CTP in differentiating between benign and malignant SPN lesions³⁹. Moreover, it is reportedly useful in the histological differentiation between adenocarcinoma (AC) and squamous cell carcinoma, thereby indicating greater benefits of anti-angiogenic treatment in patients with AC⁴⁰. Researchers have also mentioned the usefulness of CTP as a predictor of efficacy and a biomarker of the effects of anti-angiogenic therapy in the treatment of sarcoma¹⁸, non-small cell lung cancer⁴¹, pancreatic cancer⁴² and colorectal cancer⁴³.

However, CTP is a dynamic examination that requires multiple scans and is associated with a high dose of absorbed radiation. The expected dose in CTP with a satisfactory signal-to-noise ratio is a maximum of 20 mSv or 30 mSv for a tissue volume of 4 cm in or larger volumes, respectively²⁴.

The as low as reasonably achievable (ALARA) rule recommends limiting the patient's exposure to ionizing radiation to the necessary level, such that the benefits of the study outweigh the risk of side effects. The low

average dose of absorbed radiation denotes the potential of DECT modality in comparison to CTP in the context of ALARA principle, and was 4.84 mSv—meaning about 50% of CTP dose in the present study (9.07 mSv).

The differences in radiation dose between those two modalities could be much higher, even if the effective radiation dose of CTP is as low as possible. Zhu et al.³⁶ using a low-dose CTP achieved the effective radiation dose 4.67 ± 0.26 mSv vs 0.32 ± 0.10 mSv in DECT. Moreover DECT in comparison to CTP is much less dependant on the maximum length of examination in z-axis and respiratory mobility during procedure.

The DECT modality could be included in the assessment of tumor staging, with the simultaneous assessment of the effectiveness of oncological treatment based on the use of IC maps instead of BV and BF. The latter correlate with the biomarkers of MVD and VEGF angiogenesis and indicate the degree of response to anti-angiogenic therapy in neoplastic diseases. A positive response to treatment was denoted by a decrease in both values, i.e., BV and BF in the CTP study. In contrast, in the arterial phase of DECT, it corresponded to a decrease in iodine concentration in the lesion⁴⁴.

Our study had some significant limitations. First, we included a small sample size. Second, respiratory mobility during the dynamic 1-min CTP scan could be minimized, but not completely avoided. Additionally CTP in our 64-row scanner (a very common type of scanner in Polish hospitals) covered only 4 cm of length in z-axis. For those two reasons 13 patients of the study group were eliminated: 6 patients because of respiratory mobility and 7 patients because of lack of reliable perfusion data. Another restriction applied to different ROIs that were manually inserted. Therefore, they did not reflect identical places on the perfusion and DECT maps. Finally, lack of patients undergoing anti-angiogenic oncological treatment during the analysis was also a limitation. Despite these limitations, we obtained high reproducibility of the measurements as assessed by the ICC test. Notably, tumor heterogeneity is a natural limitation of both techniques.

Conclusions

Our long-term goal was to use the DECT modality in the CT oncology protocol. We believe that using DECT could be particularly beneficial in assessing tumors that display an apparent growth that is in fact caused by e.g. hemorrhage associated with anti-angiogenic treatment. The Response Evaluation Criteria in Solid Tumors (RECIST 1.1) and modified RECIST 1.1 for immune-based therapeutics (iRECIST)⁴⁵ are based on the measurement of the size of lesion. Using RECIST, such tumors would be described as progressing^{46,47}, however DECT imaging could make it possible to differentiate such changes from actual tumor growth⁴⁸. Such modification of the oncology protocol could have significant implications in further patient management.

In conclusion, the results of our study highlighted the usefulness of DECT in the assessment of functional changes in the tumor vascular bed. Although it requires further studies, DECT examination could possibly replace CTP in the future in the functional assessment of oncological changes during early diagnosis and monitoring the effects of treatment, with comparatively lower exposure to the effects of radiation.

Data availability

Datasets generated analysed during the current study are not publicly available due to personal data protections laws, however they can be made available from the author on a reasonable request (in anonymized form). In such cases, please contact dr Arkadiusz Zegadło (azegadlo@wim.mil.pl).

Received: 21 May 2022; Accepted: 28 December 2022

Published online: 04 January 2023

References

1. Wild, C. P. & Stewart, B. W. World Cancer Report 2014, n.d. <http://publications.iarc.fr/Non-Series-Publications/World-Cancer-Reports/World-Cancer-Report-2014> (accessed 25 Nov 2018).
2. Zhao, S.-J. & Wu, N. Early detection of lung cancer: Low-dose computed tomography screening in China, Thoracic. *Cancer* **6**, 385–389. <https://doi.org/10.1111/1759-7714.12253> (2015).
3. Henzler, T., Schmid-Bindert, G., Fink, C. Pulmonary nodules and lung cancer. In *Dual Energy CT in Clinical Practice* (eds. Johnson, T., Fink, C., Schönberg, S. O., Reiser, M. F.) 101–109 (Springer, 2011). https://doi.org/10.1007/174_2010_53.
4. Wang, G., Zhang, C., Li, M., Deng, K. & Li, W. Preliminary application of high-definition computed tomographic gemstone spectral imaging in lung cancer. *J. Comput. Assist. Tomogr.* **38**, 77. <https://doi.org/10.1097/RCT.0b013e3182a21633> (2014).
5. Swensen, S. J., Brown, L. R., Colby, T. V. & Weaver, A. L. Pulmonary nodules: CT evaluation of enhancement with iodinated contrast material. *Radiology* **194**, 393–398. <https://doi.org/10.1148/radiology.194.2.7824716> (1995).
6. Swensen, S. J. et al. Solitary pulmonary nodule: CT evaluation of enhancement with iodinated contrast material—A preliminary report. *Radiology* **182**, 343–347. <https://doi.org/10.1148/radiology.182.2.1732947> (1992).
7. Zhang, M. & Kono, M. Solitary pulmonary nodules: Evaluation of blood flow patterns with dynamic CT. *Radiology* **205**, 471–478. <https://doi.org/10.1148/radiology.205.2.9356631> (1997).
8. Zieliński, K. W., Kulig, A. & Zieliński, J. Morphology of the microvascular bed in primary human carcinomas of lung: Part II morphometric investigations of microvascular bed of lung tumors. *Pathol. Res. Pract.* **178**, 369–377. [https://doi.org/10.1016/S0344-0338\(84\)80029-1](https://doi.org/10.1016/S0344-0338(84)80029-1) (1984).
9. Zieliński, K. W. & Kulig, A. Morphology of the microvascular bed in primary human carcinomas of lung: Part I: Three-dimensional pattern of microvascular network. *Pathol. Res. Pract.* **178**, 243–250. [https://doi.org/10.1016/S0344-0338\(84\)80106-5](https://doi.org/10.1016/S0344-0338(84)80106-5) (1984).
10. Milne, E. N. C. Circulation of primary and metastatic pulmonary neoplasms. *Am. J. Roentgenol.* **100**, 603–619. <https://doi.org/10.2214/ajr.100.3.603> (1967).
11. Viallard, C. & Larrivé, B. Tumor angiogenesis and vascular normalization: Alternative therapeutic targets. *Angiogenesis* **20**, 409–426. <https://doi.org/10.1007/s10456-017-9562-9> (2017).
12. Li, Y. et al. Whole tumour perfusion of peripheral lung carcinoma: Evaluation with first-pass CT perfusion imaging at 64-detector row CT. *Clin. Radiol.* **63**, 629–635. <https://doi.org/10.1016/j.crad.2007.12.012> (2008).
13. Li, Y. et al. Peripheral lung carcinoma: Correlation of angiogenesis and first-pass perfusion parameters of 64-detector row CT. *Lung Cancer* **61**, 44–53. <https://doi.org/10.1016/j.lungcan.2007.10.021> (2008).

14. Ma, S.-H. *et al.* Peripheral pulmonary nodules: Relationship between multi-slice spiral CT perfusion imaging and tumor angiogenesis and VEGF expression. *BMC Cancer* **8**, 186. <https://doi.org/10.1186/1471-2407-8-186> (2008).
15. Miles, K. A. Functional computed tomography in oncology. *Eur. J. Cancer* **38**, 2079–2084. [https://doi.org/10.1016/S0959-8049\(02\)00386-6](https://doi.org/10.1016/S0959-8049(02)00386-6) (2002).
16. Miles, K. A. & Griffiths, M. R. Perfusion CT: A worthwhile enhancement?. *BJR*. **76**, 220–231. <https://doi.org/10.1259/bjr/13564625> (2003).
17. Zhu, A. X., Holalkere, N. S., Muzikansky, A., Horgan, K. & Sahani, D. V. Early antiangiogenic activity of bevacizumab evaluated by computed tomography perfusion scan in patients with advanced hepatocellular carcinoma. *Oncologist* **13**, 120–125. <https://doi.org/10.1634/theoncologist.2007-0174> (2008).
18. Kambadakone, A. *et al.* CT perfusion as an imaging biomarker in monitoring response to neoadjuvant bevacizumab and radiation in soft-tissue sarcomas: Comparison with tumor morphology, circulating and tumor biomarkers, and gene expression. *Am. J. Roentgenol.* **204**, W11–W18. <https://doi.org/10.2214/AJR.13.12412> (2014).
19. Bai, R. *et al.* Solitary pulmonary nodules: Comparison of multi-slice computed tomography perfusion study with vascular endothelial growth factor and microvessel density. *Chin. Med. J.* **122**, 541–547 (2009).
20. Goh, V. *et al.* Radiation dose from volumetric helical perfusion CT of the thorax, abdomen or pelvis. *Eur. Radiol.* **21**, 974–981. <https://doi.org/10.1007/s00330-010-1997-y> (2011).
21. Chen, X. *et al.* Correlation of iodine uptake and perfusion parameters between dual-energy CT imaging and first-pass dual-input perfusion CT in lung cancer. *Medicine (Baltimore)* **96**, e7479–e7479. <https://doi.org/10.1097/MD.0000000000007479> (2017).
22. Gordic, S. *et al.* Correlation between dual-energy and perfusion CT in patients with hepatocellular carcinoma. *Radiology* **280**, 78–87. <https://doi.org/10.1148/radiol.2015151560> (2016).
23. Kang, H. J., Kim, S. H., Bae, J. S., Jeon, S. K. & Han, J. K. Can quantitative iodine parameters on DECT replace perfusion CT parameters in colorectal cancers?. *Eur. Radiol.* **28**, 4775–4782. <https://doi.org/10.1007/s00330-0-18-5502-3> (2018).
24. Miles, K. A. *et al.* on behalf of the Experimental Cancer Medicine Centre Imaging Network Group. Current status and guidelines for the assessment of tumour vascular support with dynamic contrast-enhanced computed tomography. *Eur. Radiol.* **22**, 1430–1441. <https://doi.org/10.1007/s00330-012-2379-4> (2012).
25. Schober, P., Boer, C. & Schwarte, L. A. Correlation coefficients: Appropriate use and interpretation. *Anesth. Analg.* **126**, 1763–1768 (2018).
26. Zegadlo, A. *et al.* Assessment of solitary pulmonary nodules based on virtual monochrome images and iodine-dependent images using a single-source dual-energy CT with fast kVp switching. *J. Clin. Med.* **9**, E2514. <https://doi.org/10.3390/jcm9082514> (2020).
27. Zhang, Y. *et al.* Can spectral CT imaging improve the differentiation between malignant and benign solitary pulmonary nodules?. *PLoS One*. **11**, e0147537. <https://doi.org/10.1371/journal.pone.0147537> (2016).
28. Xu, X. *et al.* Clinical utility of quantitative dual-energy CT iodine maps and CT morphological features in distinguishing small-cell from non-small-cell lung cancer. *Clin. Radiol.* **74**, 268–277. <https://doi.org/10.1016/j.crad.2018.10.012> (2019).
29. Geyer, L. L. *et al.* Imaging of acute pulmonary embolism using a dual energy CT system with rapid kVp switching: Initial results. *Eur. J. Radiol.* **81**, 3711–3718. <https://doi.org/10.1016/j.ejrad.2011.02.043> (2012).
30. Kikano, E. G. *et al.* Pulmonary embolism versus mimics on dual-energy spectral computed tomography: An algorithmic approach. *J. Comput. Assist. Tomogr.* **44**, 833–840 (2020).
31. Vlahos, I., Jacobsen, M. C., Godoy, M. C., Stefanidis, K. & Layman, R. R. Dual-energy CT in pulmonary vascular disease. *Br. J. Radiol.* **95**, 20210699. <https://doi.org/10.1259/bjr.20210699> (2022).
32. Martini, K. & Frauenfelder, T. Emphysema and lung volume reduction: The role of radiology. *J. Thorac. Dis.* **10**, S2719–S2731. <https://doi.org/10.21037/jtd.2018.05.117> (2018).
33. Moon, J. W. *et al.* Perfusion- and pattern-based quantitative CT indexes using contrast-enhanced dual-energy computed tomography in diffuse interstitial lung disease: Relationships with physiologic impairment and prediction of prognosis. *Eur. Radiol.* **26**, 1368–1377. <https://doi.org/10.1007/s00330-015-3946-2> (2016).
34. Mulé, S. *et al.* Can dual-energy CT replace perfusion CT for the functional evaluation of advanced hepatocellular carcinoma?. *Eur. Radiol.* **28**, 1977–1985. <https://doi.org/10.1007/s00330-017-5151-y> (2018).
35. Skornitzke, S. *et al.* Dual-energy CT iodine maps as an alternative quantitative imaging biomarker to abdominal CT perfusion: Determination of appropriate trigger delays for acquisition using bolus tracking. *BJR*. **91**, 20170351. <https://doi.org/10.1259/bjr.20170351> (2018).
36. Zhu, B., Zheng, S., Jaing, T. & Hu, B. Evaluation of dual-energy and perfusion CT parameters for diagnosing solitary pulmonary nodules. *Thorac. Cancer*. **12**, 2691–2697 (2021).
37. Folkman, J. Tumor angiogenesis: Therapeutic implications. *N. Engl. J. Med.* **285**, 1182–1186. <https://doi.org/10.1056/NEJM19711118285210> (1971).
38. Yang, H. F. *et al.* Perfusion computed tomography evaluation of angiogenesis in liver cancer. *Eur. Radiol.* **20**, 1424–1430. <https://doi.org/10.1007/s00330-009-1693-y> (2010).
39. Yuan, X. *et al.* Differentiation of malignant and benign pulmonary nodules with first-pass dual-input perfusion CT. *Eur. Radiol.* **23**, 2469–2474. <https://doi.org/10.1007/s00330-013-2842-x> (2013).
40. Zhang, Z. *et al.* A single enhanced dual-energy CT scan may distinguish lung squamous cell carcinoma from adenocarcinoma during the venous phase. *Acad. Radiol.* **27**, 624–629. <https://doi.org/10.1016/j.acra.2019.07.018> (2020).
41. Wang, J., Wu, N., Cham, M. D. & Song, Y. Tumor response in patients with advanced non-small cell lung cancer: Perfusion CT evaluation of chemotherapy and radiation therapy. *Am. J. Roentgenol.* **193**, 1090–1096. <https://doi.org/10.2214/AJR.08.1367> (2009).
42. Park, M.-S. *et al.* Perfusion CT: Noninvasive surrogate marker for stratification of pancreatic cancer response to concurrent chemotherapy and radiation therapy. *Radiology* **250**, 110–117. <https://doi.org/10.1148/radiol.2493080226> (2009).
43. Bellomi, M., Petralia, G., Sonzogni, A., Zampino, M. G. & Rocca, A. CT perfusion for the monitoring of neoadjuvant chemotherapy and radiation therapy in rectal carcinoma: Initial experience. *Radiology* **244**, 486–493. <https://doi.org/10.1148/radiol.2442061189> (2007).
44. Goh, V., Ng, Q. S. & Miles, K. Computed tomography perfusion imaging for therapeutic assessment: Has it come of age as a biomarker in oncology?. *Investig. Radiol.* **47**, 2–4 (2012).
45. Seymour, L. *et al.* iRECIST: Guidelines for response criteria for use in trials testing immunotherapeutics. *Lancet Oncol.* **18**(3), e143–e152. [https://doi.org/10.1016/S1470-2045\(17\)30074-8](https://doi.org/10.1016/S1470-2045(17)30074-8) (2017) (Epub 2017 Mar 2).
46. Katz, S. I. *et al.* Radiologic pseudoprogression during anti-PD-1 therapy for advanced non-small cell lung cancer. *J. Thorac. Oncol.* **13**(7), 978–986. <https://doi.org/10.1016/j.jtho.2018.04.010> (2018) (Epub 2018 May 5).
47. Reckamp, K. L. Real-world pseudoprogression: An uncommon phenomenon. *J. Thorac. Oncol.* **13**(7), 880–882. <https://doi.org/10.1016/j.jtho.2018.05.011> (2018).
48. Kim, Y. *et al.* Dual-energy CT in patients treated with anti-angiogenic agents for non-small lung cancer: New method of monitoring tumor response?. *Korean J. Radiol.* **13**(6), 702–710. <https://doi.org/10.3348/kjr.2012.13.6.702> (2012).

Author contributions

A.Z. designed and planned the study. A.Z., M.Ž., A.M. and A.R. participated in the data collection. A.Z., E.W.-S. and A.R. performed data analysis. A.Z. and M.Ž. drafted the manuscript. All authors revised and reviewed the manuscript, as well as approved the final version of the manuscript.

Competing interests

The authors declare no competing interests.

Additional information

Correspondence and requests for materials should be addressed to A.R.

Reprints and permissions information is available at www.nature.com/reprints.

Publisher's note Springer Nature remains neutral with regard to jurisdictional claims in published maps and institutional affiliations.



Open Access This article is licensed under a Creative Commons Attribution 4.0 International License, which permits use, sharing, adaptation, distribution and reproduction in any medium or format, as long as you give appropriate credit to the original author(s) and the source, provide a link to the Creative Commons licence, and indicate if changes were made. The images or other third party material in this article are included in the article's Creative Commons licence, unless indicated otherwise in a credit line to the material. If material is not included in the article's Creative Commons licence and your intended use is not permitted by statutory regulation or exceeds the permitted use, you will need to obtain permission directly from the copyright holder. To view a copy of this licence, visit <http://creativecommons.org/licenses/by/4.0/>.

© The Author(s) 2023